

ENHANCING THE PERFORMANCE OF SLENDER STRUCTURES WITH GEOMETRIC CONSTRAINTS: A CASE STUDY WITH THE ROORDA FRAME

Lichang Zhu¹, Jiajia Shen^{1,2}, Rainer M.J. Groh¹, Mark Schenk¹ & Alberto Pirrera¹

¹Bristol Composites Institute (BCI), School of Civil, Aerospace & Design Engineering, University of Bristol, Bristol BS8 1TR, UK

²Exeter Technologies Group (ETG), Department of Engineering, University of Exeter, Exeter EX4 4QF, UK

Abstract

In the realm of structural engineering, buckling has traditionally been seen as a failure mechanism. More recently, this paradigm has shifted following the realisation that "well-behaved" geometrically nonlinear responses can be fostered to enhance load-carrying capacity and/or add functionality. This paper contributes to this evolving paradigm by applying *modal nudging* to structures with constrained geometries, such as wing panels, exemplified through a case study on Roorda frames. We introduce a shape optimisation strategy that leverages prior knowledge of post-buckling behaviour and aligns equilibrium paths with the enhanced load-displacement response of modal-nudged counterparts. This method aims to enhance structural efficiency and mitigate the risk of instability, while demonstrating the potential to reduce computational costs through a two-step optimisation process.

Keywords: Bifurcations; Well-behaved nonlinear structures; Modal nudging; Shape optimisation; Mode switching

1. Introduction

Traditionally, engineers consider the onset of geometric nonlinearites or buckling instabilities as failure modes. This approach is particularly prudent for unstable/subcritical buckling scenarios, where conservative knock-down factors are employed to prevent instabilities [1, 2]. However, a paradigm shift is emerging for stable/supercritical buckling. In these cases, researchers are exploring the potential to harness geometric nonlinearities and instabilities to create novel functionalities. This strategy opens doors for the design of advanced structures with features like programmable responses [3, 4, 5, 6, 7, 8] and morphing capabilities [9, 10, 11, 12].

Thin-walled structures are ideal candidates for exploiting buckling instabilities due to their inherent flexural compliance in the out-of-plane direction. Some thin-walled structures, such as axially-compressed cylindrical shells, exhibit unstable buckling and are highly sensitive to imperfections. In these cases, transitioning their behaviour from unstable and imperfection-sensitive to stable and imperfection-insensitive can lead to significant functional improvements. Several approaches have been explored to achieve this goal. For example, Mang *et al.* [13] and Schranz *et al.* [14] controlled snap-through behaviour of a curved plate by adding auxiliary members, like springs. Ning and Pellegrino [15] crafted a cylinder with a corrugated wall to make it imperfection insensitive. White and Weaver [16] designed a composite cylindrical panel with curvilinear reinforcing fibres that removes imperfection sensitivity. While effective, these nonlinear elastic tailoring methods often necessitate substantial structural modifications.

Another approach to elastic tailoring involves introducing controlled geometric modifications, known as engineered imperfections, to ensure they dominate the effects of any random imperfections that might be present. This method offers a significant advantage: achieving a tailored structural response

often requires only minor alterations to the original geometry. Formal optimisation techniques can be employed to identify these engineered imperfections. For instance, Burgueno *et al.* [17] used an optimiser to find a superposition of eigenmodes to control the number of mode jumps and the post-buckling load drop in a cylindrical shell. Similarly, Liguori *et al.* [18] utilised a Monte Carlo optimiser with a reduced-order model to identify engineered imperfections that reduce imperfection sensitivity. Notably, both these optimisation-based approaches do not require prior knowledge of the structure's post-buckling behaviour.

In contrast to optimisation methods, seeded imperfections can also be identified analytically through an approach known as *modal nudging* [19, 20]. This method leverages knowledge of post-buckling behaviour, obtained using a generalised path-following method [21]. The key idea is to identify a stable post-buckling mode shape with a higher load-carrying capacity that is inaccessible from the structure's natural loading path. Even though unreachable under normal loading, this mode shape can be used as a target for the engineered imperfection: by introducing a scaled-down version of this target shape as a geometric modification, modal nudging enables the structure to reach the previously inaccessible stable configuration. The advantage of modal nudging is the interpretability and determinism. By utilising prior knowledge of the post-buckling behaviour, the modification of the original geometry becomes intentional and predictable. Additionally, the asymptotic convergence of perturbed equilibrium paths to the perfect behaviour allows for a prior knowledge of the perturbed structure's performance.

While modal nudging and other nonlinear elastic tailoring methods offer promising results, they often modify the geometry on both sides of a thin-walled structure. However, many practical applications involve structures with constraints on one surface — for instance, aerodynamic constraints on the outer surface of an aeroplane wing panel. This work addresses this challenge by extending the concept of modal nudging to structures with geometric constraints. We explore a novel method called thickness nudging, which modifies the thickness profile on the unconstrained side of the structure to achieve the desired stability improvements. This approach offers a significant advantage: it allows for targeted stability enhancement while maintaining the integrity of the constrained surface. However, modifying the thickness on one side can affect the overall behaviour of the structure due to changes in flexural rigidity. To address this complexity, we introduce an optimisation algorithm with a novel pathaligning objective. This strategy guides the optimisation process to achieve the target post-buckling nonlinear equilibrium path identified through modal nudging. Consequently, the optimisation method achieves the same enhancements in load-carrying capacity as modal nudging, while satisfying the desired geometric constraints.

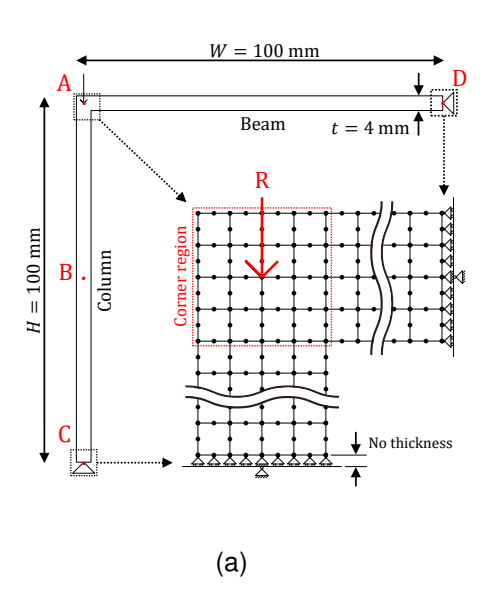
The structure of this paper is as follows: Section 2 details the problem definition and methods. Section 3 presents the numerical results and discussions. The paper concludes with Section 4, summarising the key findings and their implications in structural engineering.

2. Problem Description and Methods

2.1 Roorda frame

The Roorda frame shown in Figure 1a is adopted as the case study for our work. The frame consists of a vertical member ('column') rigidly connected to a horizontal member ('beam') at the junction. The frame is supported via two pinned connections, and is loaded with a vertical downwards force at the beam—column junction (Point A). The Roorda frame is a well-established benchmark in nonlinear mechanics due to its characteristic post-buckling behaviour, and is here selected particularly for the presence of an isolated stable path with the potential for increased load-carrying capacity; see Figure 1b. Additionally, the frame features distinct 'outside' and 'inside' surfaces, ideally for demonstrating the application of geometric constraints.

The Roorda frame has a uniform thickness t of 4 mm, height H of $100 \, \mathrm{mm}$ and width W of $100 \, \mathrm{mm}$. It is made of aluminium with a Young's modulus $E = 70 \, \mathrm{GPa}$, Poisson ratio v = 0.25 and yield stress $\sigma_{\mathrm{Y}} = 280 \, \mathrm{MPa}$. The finite element (FE) model is discretised using 8-node biquadratic plane stress elements with reduced integration (CPS8R), which can effectively avoid hourglassing. Uniform and structured mesh scheme is adopted and the size of the element is 1 mm, *i.e.* 4 elements through the thickness of the column/beam. The chosen mesh size is based on a mesh sensitivity study. A



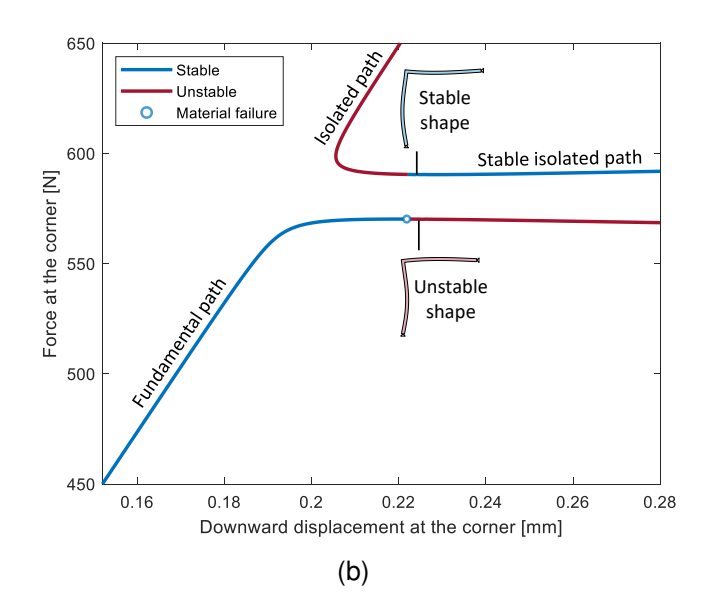


Figure 1 – (a) The baseline Roorda frame [22] loaded under a vertical downwards force at Point A. The dimensions of the frame are optimised based on the condition that material failure and structural instability occur simultaneously. (b) The equilibrium manifold with deformation modes. Stability failure is indicated by a blue path becoming red. Material failure is denoted by the blue circle. The stable isolated path provides a higher load-carrying capacity, but it is disconnected from the natural loading path.

vertical concentrated load *R* is applied at the centre of the junction region, as shown in Figure 1a. The *von Mises* criterion is used to evaluate material failure, with the exclusion of the corner region due to unrealistic stresses at the loading point. Figure 1a illustrates the boundary conditions implemented to prevent stress concentration. The Rigid Body option in ABAQUS is used to constrain the end-sections to reference points, which allows the boundary nodes to rotate along virtual planes pivoting around the central nodes, mimicking pinned connections. The Riks (arc-length) solver [23] is used to solve the nonlinear equilibrium paths of the frame. The stability of the structure is evaluated by monitoring the number of negative eigenvalues in the tangential stiffness matrix at the converged equilibria, which is output in ABAQUS' default output '.msg' file.

Figure 1b presents the equilibrium manifold for the Roorda frame, where the applied force is plotted against the corresponding vertical displacement at Point A. The pristine (unmodified) Roorda frame follows the fundamental path: the force-displacement response is roughly linear until the structure rapidly softens when the column bends towards the right. The frame subsequently loses stability at the force limit point. We designed the Roorda frame such that stability loss and material failure occur simultaneously, resulting in an optimal design with no redundancy. The failure load of 570 N serves as the baseline performance for this structure. The isolated path, with its higher load-carrying capacity compared to the fundamental path, was solved using a multi-step analysis approach [21]. Firstly, the Roorda frame was loaded into the post-buckling regime. Then, a perturbation force was applied at the mid-height of the column, forcing it to deflect leftwards. Once the desired deflection was achieved, the perturbation force was removed, allowing the frame to stabilise on the isolated path. Finally, the Riks solver was used to trace the entire isolated path by gradually reducing the vertical force. This isolated path contains a stable segment, which has a higher load-carrying capacity than the fundamental path. The deformation profile of the frame on this isolated stable segment is utilised in the next section for the application of elastic tailoring methods.

2.2 Elastic tailoring methods

In this section, we explore three methods to increase load-carrying capacity and remove instability of the Roorda frame. We aim to achieve these improvements, utilising minimal geometric modifications from the existing 'optimum' design (where material and stability failure occur simultaneously). We will

detail these three methods, alongside their effectiveness in achieving the desired outcomes.

2.2.1 Modal Nudging

Modal nudging exploits the knowledge of the Roorda frame's post-buckling response. A deformed configuration is selected from the start of the stable segment of the isolated path as shown in Figure 1b. Its displacement vector, $\mathbf{u}_{\text{state}}$, is then normalised by $\|\mathbf{u}_{\text{state}}\|_2$ and scaled by a non-dimensional nudging parameter η and seeded into the undeformed geometry of the pristine Roorda frame, \mathbf{x}_0 . Hence.

$$\mathbf{x}_{\mathsf{nudged}} = \mathbf{x}_0 + \eta \bar{\mathbf{u}}_{\mathsf{state}},$$
 (1)

with

$$\bar{u}_{\text{state}} = \frac{u_{\text{state}}}{\|u_{\text{state}}\|_2},$$
(2)

and

$$\eta \| \bar{\boldsymbol{u}}_{\text{state}} \oslash \boldsymbol{\mathsf{x}}_0 \|_2 \ll 1,$$
 (3)

where \oslash is the Hadamard division operator defined by $C_i = A_i/B_i$ with i being the number ith component of the vector.

Figure 2a-i shows five modal-nudged Roorda frames, with resulting equilibrium paths in Figure 2a-ii. A minimum value of $\eta=0.00440$ is required to bridge the gap between the fundamental and isolated paths — this is the 'critically nudged' configuration shown in Frame 1. As the nudging parameter is increased, the performance degrades (reduced initial stiffness and/or lower post-buckling capacity) and can fall below that of the baseline response. For example, Frame 3 exhibits an improved failure load; however, its equilibrium path falls below the fundamental path at approximately $560~\rm N$, indicating that it deforms more than the baseline at this load. In contrast, the equilibrium paths of Frames 1 and 2 are entirely above the fundamental path, making them suitable for minimising deformation under all loading conditions. When the nudge failure load is below the baseline, such as for Frames 4 and 5, the configuration is considered 'overly nudged'.

2.2.2 Thickness Nudging

In this section, we consider a more intricate applications of modal nudging, where geometric constraints exists, such as wing skin panels with a defined aerodynamic profile. Illustrated in Figure 2b-i, the outer profile of the Roorda frame is deliberately constrained, while the inner profile is manipulated through the nudging process. Thickness nudging involves constraining the outer geometry, with the nudge altering the neutral axis of the Roorda frame's beam and column—thereby defining the frame's inner profile. After thickness nudging, the column becomes thinner at mid-height, and the beam thickens at mid-span to align the neutral axis with that of the post-buckling shape. The inherent coupling between the change in the neutral axis and the subsequent redistribution of stiffness presents a challenge for thickness nudging. This complexity can potentially hinder the ability to attain the optimal structural response. Figure 2b-i shows the thickness-nudged Roorda frames with their equilibrium paths in Figure 2b-ii. Although the thickness-nudged path can offer an improvement over the baseline design, the equilibrium paths are not asymptotic to the stable isolated path and therefore do not reach the full potential of the structure. Thickness nudging reduces the thickness of the member in compression (column), removing instabilities at the expense of column strength. This inherent contradiction suggests the existence of a more optimal solution.

2.2.3 Shape optimisation

To exploit the full potential of the Roorda frame, we employ shape optimisation to identify seeded imperfections that can bridge the fundamental path to the desirable stable isolated path. However, successful optimisation requires a careful selection of objective function, constraints, FE solvers and optimisation algorithms.

The outer geometry of the Roorda frames and their thickness at the supporting boundaries remain fixed, whilst the inner surface is allowed to vary. The inner surface is parameterised through a series of evenly spaced control points. These control points allow for independent vertical movement on the beam and horizontal movement on the column. From these control points, two smooth curves

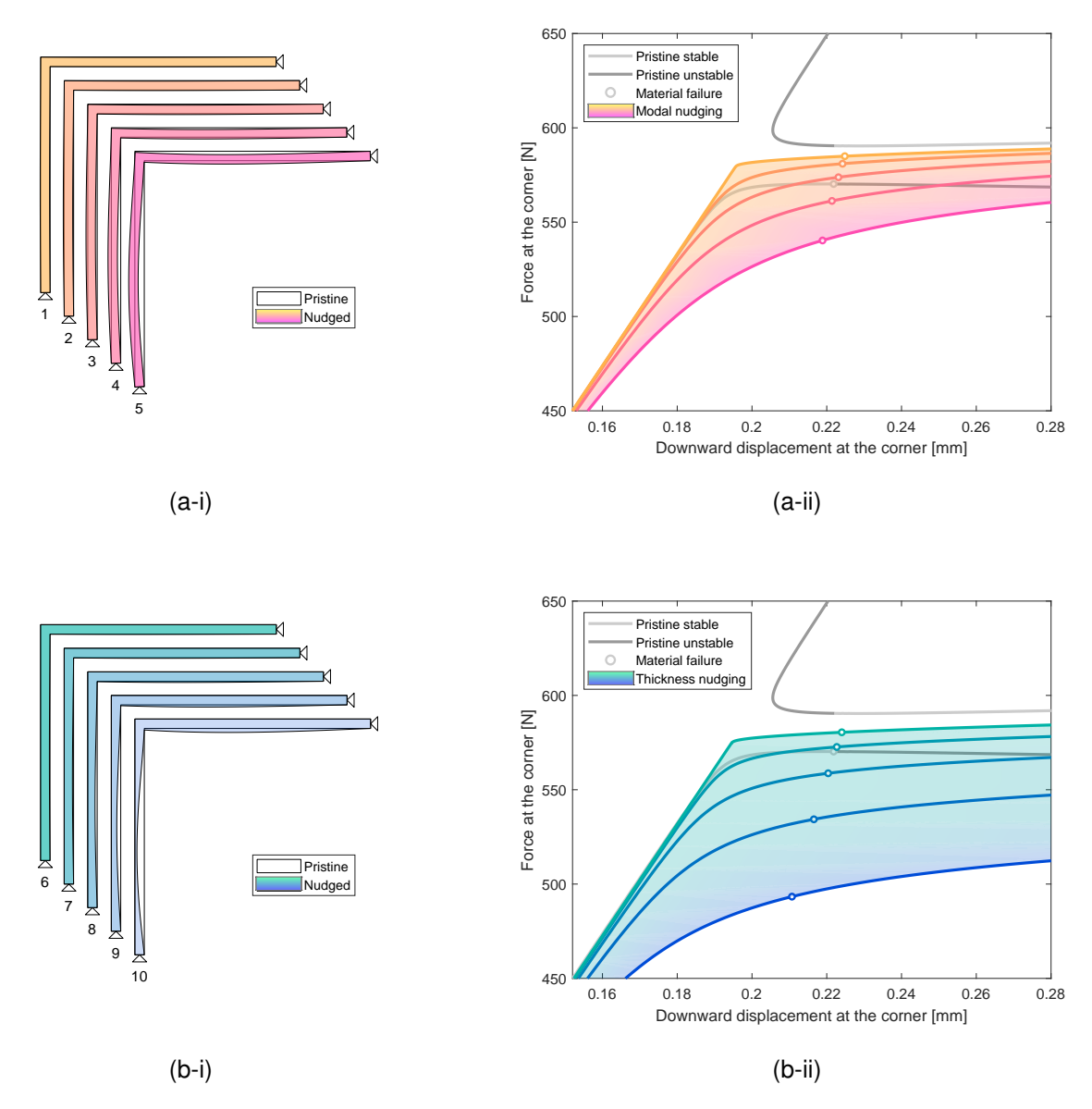


Figure 2 – (a-i) Modal-nudged Roorda frames, ranging from critically nudged (Frame 1, $\eta=0.00440$) to overly nudged (Frame 5, $\eta=0.05274$). The nudged configurations are scaled 25× to visualise the engineered imperfections. (a-ii) The equilibrium paths of the nudged frames are overlaid on the pristine equilibrium manifold. The point of material failure is indicated by a circular marker on the equilibrium path. The nudged paths remain stable and converge asymptotically to the stable isolated path. (b-i) Thickness-nudged Roorda frames (15× scaled engineered imperfection) from critically nudged (Frame 6, $\eta=0.00443$) to overly nudged (Frame 10, $\eta=0.05274$). (b-ii) The corresponding equilibrium paths do not converge to the stable isolated path, and have a lower load-carrying capacity.

are generated using the Modified Akima Interpolation method [24]. This method offers a distinct advantage over spline interpolation by preventing overshoots that could create notches and weaken the structure. A convergence study showed that increasing the number of control points from 4 to 14 led to performance convergence.

In contrast to traditional structural optimisation, which often focuses on maximising the failure load while minimising mass, our optimisation strategy explicitly exploits prior knowledge of the post-buckling response. Consequently, we propose an unconventional objective function: aligning the equilibrium path of the optimised structure to that of the modal-nudged structure. This is achieved by minimising the average distance D_{paths} (in load-displacement space) between the target path and the optimising path,

$$D_{\mathsf{paths}} = \frac{1}{S} \int_0^S \sqrt{(v(s) - v_{\mathsf{t}}(s))^2 + (R(s) - R_{\mathsf{t}}(s))^2} \, ds,\tag{4}$$

where R is the vertical load at Point A, v is the corresponding vertical displacement, and subscript t denotes the target path. The variables are parameterised as function of arc-length s, and s is the arclength when $v_t = 1 \, \mathrm{mm}$. The path-aligning objective is practical and attainable, as it targets equilibrium paths known to be achievable with insignificant geometric alterations. Further, both material and stability failures are considered by minimising the distance D_{failure} between the material failure point on the target path and the first failure point (whether material or stability failure) on the optimising path,

$$D_{\text{failure}} = \sqrt{(v_{\text{m}} - v_{\text{mt}})^2 + (R_{\text{m}} - R_{\text{mt}})^2},$$
 (5)

where $(\nu_{\rm m},R_{\rm m})$ and $(\nu_{\rm mt},R_{\rm mt})$ are the failure points on the optimising path and target paths. Lastly, we exploit our insight into the desired post-buckling response by implementing constraints on the post-buckling translations and rotations of Points A-D. By excluding infeasible areas of the design space, these constraints expedite the initial phase of the optimisation process.

The combined objectives are therefore to align equilibrium paths, match failure load and displacement, and minimise volume (and thus mass), subject to constraints on displacements and rotations of specific points on the structure:

$$\begin{aligned} & \underset{\boldsymbol{x}_{c}}{\min} & \frac{V}{V_{0}} \left(1 + 100 \cdot D_{\text{failure}}\right) \left(1 + 100 \cdot D_{\text{paths}}\right) \\ & \text{s.t.} & A_{v} < 0 & \text{(Point A must move downwards)} \\ & B_{u} < 0 & \text{(Point B must move leftwards)} \\ & C_{a} < 0 & \text{(Point C must rotate counterclockwise)} \\ & D_{a} < 0 & \text{(Point D must rotate counterclockwise)} \end{aligned}$$

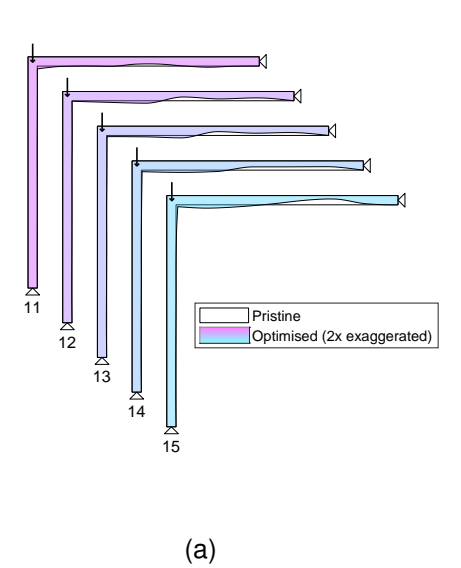
where x_c is the deviation displacement of the control points from the baseline; V and V_0 are the optimising volume and the original volume of the Roorda frame, respectively. In the objective function, D_{failure} and D_{paths} are scaled by a factor 100 to match the magnitude of V/V_0 .

The modal-nudged and thickness-nudged Roorda frames exhibit two potential post-buckling shapes, determined by the size of the nudging parameter relative to the critical value. The stable post-buckling response is structurally more efficient, resulting in a higher objective score than the unstable shape. This step change in the objective score at the critical nudging parameter suggests that the objective landscape may contain discontinuities, making it unsuitable for gradient-based optimisation. Therefore, we use the gradient-free, surrogate optimiser (surrogateopt) in MATLAB, which is suited to navigate the complexities of this scenario.

3. Results and Discussion

3.1 Modal Nudging and Thickness Nudging

Figure 2a-i/ii show the configuration of five modal-nudged frames alongside their corresponding equilibrium paths. Their performance are summarised in Table 1. All modal-nudged frames remain stable throughout their equilibrium path, successfully connecting the fundamental path (pre-buckling) to the stable isolated path (post-buckling). The equilibrium path of Frames 1 and 2 remains entirely



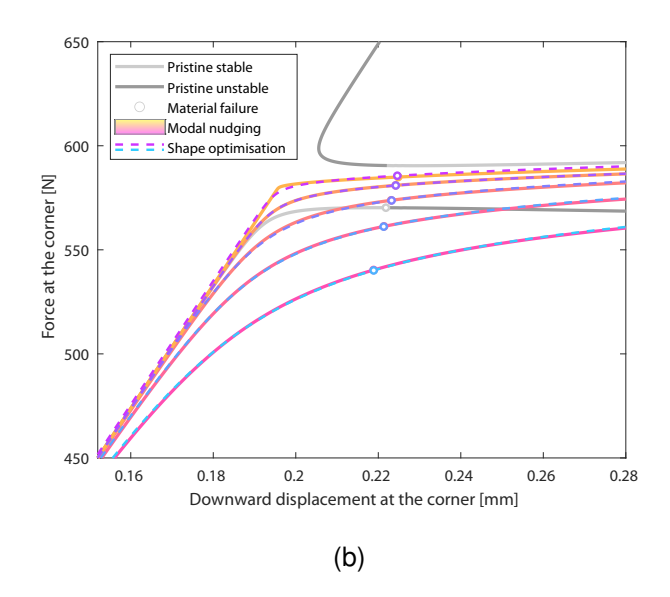


Figure 3 – (a) Shape-optimised Roorda frames (2× exaggerated deformation) from critically nudged (Frame 11) to overly nudged (Frame 15). The optimiser works by thinning the middle of the beams, without significantly affecting the column. (b) The shape-optimised equilibrium paths (dotted lines) overlap on Figure 2a-ii (modal-nudged equilibrium paths). The shape-optimised equilibrium paths remain stable. The paths and material failure points (indicated by circular marker) match those of the modal-nudged ones.

above the fundamental path, indicating enhanced structural performance with minimal mass change. Frame 1, with a critical nudging parameter ($\eta=0.00440$), offers optimal performance but is potentially sensitive to adverse geometric imperfections that mimic a reduction in the nudging parameter, making it unstable with even minor imperfections. Frame 3 exhibits an increased load-carrying capacity, but its equilibrium path dips below the fundamental path, indicating reduced initial stiffness. Frames 4 and 5, categorised as 'overly nudged', display both reduced initial stiffness and load-carrying capacity. Overall, Frame 2 represents the most practical solution. It offers improvements without compromising initial stiffness and exhibits lower sensitivity to adverse geometric imperfections. Because Frame 2's nudging parameter is further from the critical value, larger imperfections are required to destabilise it, making Frame 2 less sensitive to geometric imperfections compared to Frame 1.

The thickness-nudged results are presented in Figures 2b-i and Table 1. Similar to modal nudging, all nudged frames remain stable along their equilibrium paths. Frame 6 represents the critical nudging case ($\eta=0.00443$), while frames 7–10 are categorised as overly nudged ($\eta\geq0.00823$). While thickness nudging can achieve increased performance compared to the baseline design, it appears generally less effective than modal nudging. This is evident when comparing the achievable failure load and efficiency ratio $R_{\rm fail}/V$ (i.e failure load per unit volume). Thickness nudging tends to reduce the thickness of the primary load-bearing members, leading to the equilibrium paths to converge below the target path and limiting potential improvement. Consequently, the practical range of nudging parameters for thickness nudging is narrower due to the risk of performance reduction.

3.2 Shape Optimisation

Figure 3b demonstrates that the equilibrium paths obtained through shape optimisation closely resemble those achieved via modal nudging. Frame 12, with a response matching Frame 2, emerges as the most practical solution with the highest efficiency ratio ($R_{\rm fail}/V=0.7560~{\rm N/mm^2}$) among all frames, outperforming both modal nudging and thickness nudging results. This optimised design offers a load improvement of 3.95% compared to the baseline Roorda frame.

While the equilibrium paths are very similar, Figure 3a reveals intriguing differences in the underlying mechanisms (*i.e.* geometry) between the optimised shapes and the analytically nudged frames. The pristine Roorda frame exhibits a tendency to deform into an unstable configuration due to asymmet-

rical moments in the pre-buckling regime. In this regime, the beam applies a small counter-clockwise moment to the column, breaking its symmetry and causing buckling towards the right (unstable configuration as shown in Figure 1b). Modal nudging and thickness nudging techniques address this issue by shifting the column's neutral axis leftward, generating a clockwise moment to counteract the beam's counter-clockwise moment and promote stable buckling to the left. However, since the beam is not in compression during this stage, nudging applied directly to the beam has minimal effect, rendering it somewhat irrelevant in this context. Shape optimisation tackles this challenge with a distinct approach that prioritises maintaining the desired initial stiffness of the column. The key innovation lies in stiffening the beam-column connection while incorporating a 'compliant hinge' (particularly evident in Frame 15) within the beam itself. This compliant hinge exhibits reduced flexural rigidity, reflected in the significantly higher maximum thickness change (\bar{u}/t) compared to the modal-nudged and thickness-nudged frames (refer to Table 1). As the corner point displaces downward under the applied load, the compliant hinge allows the beam to exert a crucial clockwise moment on the column, ultimately guiding it to buckle towards the left into the stable configuration.

3.3 Computational cost

Incorporating nonlinear elastic tailoring into global optimisation presents a significant computational hurdle. Compared to a separate linear optimisation process followed by modal nudging or the shape optimisation method proposed here, the computational resources required for nonlinear global optimisation are considerably higher. This stems from two key factors: 1) Solver Complexity: Nonlinear finite element (FE) solvers are significantly more computationally expensive than their linear counterparts. 2) Landscape Complexity: The objective function in a multi-modal nonlinear scenario is often riddled with challenges for gradient-based optimisation algorithms. These challenges include the presence of numerous local minima and discontinuities. Consequently, such scenarios necessitate the use of gradient-free optimisation algorithms. While these algorithms offer robustness in navigating complex landscapes, they are typically slower than their gradient-based counterparts. Furthermore, an integrated optimisation approach would require exploring a wider range of parameter variations, such as thickness and width of the Roorda frame. In contrast, the proposed shape optimisation method focuses on introducing only small thickness changes. This is because a near-optimal thickness distribution can often be pre-determined through conventional optimisation techniques. This significantly reduces the computational demands placed on nonlinear FE solvers.

4. Conclusions

In this work, we propose a shape optimisation technique to identify engineered geometric perturbations that replicate the performance benefits of modal nudging within structures constrained by a fixed outer geometry. This approach opens doors for applying modal nudging to real-world structures with complex shapes, such as wing panels. Our method leverages shape optimisation as a post-processing step following a conventional optimisation process. This strategy has the potential to significantly reduce computational costs compared to a fully nonlinear global optimisation approach. We achieve this advantage by employing a novel 'path-aligning' objective function within the shape optimisation framework. In essence, this work presents a practical tool that can mitigate the risk of instability in optimised structures with geometric constraints, paving the way for a new generation of high-performance designs.

Authors' contribution

LZ, JS, RMJG, MS and AP: Conceptualisation, Methodology. LZ: Data Writing - Original Draft, FE Model Development. JS, RMJG, MS and AP: Writing - Review & Editing, Supervision. All authors have read and approved the final manuscript.

Acknowledgments

This research was co-funded by Embraer S.A. and the UK Engineering and Physical Sciences Research Council (EPSRC) through the EPSRC Centre for Doctoral Training in Composites Science, Engineering and Manufacturing (CoSEM CDT) [Grant No. EP/S021728/1]. The support and funding

Table 1 – An overview of the performance of 15 elastically tailored Roorda frames. Nudging parameter η is the scaling factor from target mode shape to the shape of perturbation. \bar{u}/t is the maximum geometry alteration divided by thickness. $(V-V_0)/V_0$ is the change in volume divided by the original volume, a measure of the change in mass. $R_{\rm fail}/V$ is the failure load per unit volume, a measure of specific strength.

	No.	η	\bar{u}/t	$(V - V_0)/V_0$	$R_{\rm fail}$	R_{fail}/V	$\Delta R_{\rm fail}/V$
	[-]	[-]	[%]	[%]	[N]	$[N/mm^2]$	[%]
Baseline frame	0	_	_	_	570	0.7273	_
Modal nudging	1	0.00440	0.217	-0.0008	585	0.7461	+2.58
	2	0.00819	0.405	-0.0016	581	0.7410	+1.88
	3	0.01524	0.753	-0.0028	574	0.7319	+0.63
	4	0.02835	1.400	-0.0052	561	0.7159	-1.57
	5	0.05274	2.605	-0.0095	540	0.6892	-5.24
Thickness nudging	6	0.00443	0.437	-0.0509	580	0.7407	+1.84
	7	0.00823	0.811	-0.0945	573	0.7311	+0.52
	8	0.01528	1.507	-0.1755	559	0.7139	-1.84
	9	0.02839	2.800	-0.3258	534	0.6838	-5.98
	10	0.05274	5.201	-0.6050	493	0.6331	-13.0
Shape optimisation	11	_	15.28	-0.3079	586	0.7492	+3.01
	12	_	20.39	-1.9868	581	0.7560	+3.95
	13	_	20.50	-2.1411	574	0.7478	+2.82
	14	_	18.56	-2.5664	561	0.7346	+1.00
	15	_	31.62	-2.0535	540	0.7033	-3.30

is gratefully acknowledged. LZ gratefully acknowledges the financial support by the China Scholarship Council (CSC) and Embraer. JS was funded by Research Fellowship from Exeter Technologies Group at University of Exeter. RMJG was also funded by the Royal Academy of Engineering under the Research Fellowship scheme [RF\201718\17178].

5. Contact Author Email Address

Lichang Zhu: lichang.zhu@bristol.ac.uk

6. Copyright Statement

The authors confirm that they, and/or their company or organisation, hold copyright on all of the original material included in this paper. The authors also confirm that they have obtained permission, from the copyright holder of any third party material included in this paper, to publish it as part of their paper. The authors confirm that they give permission, or have obtained permission from the copyright holder of this paper, for the publication and distribution of this paper as part of the ICAS proceedings or as individual off-prints from the proceedings.

References

- [1] Castro SGP, Zimmermann R, Arbelo MA, Khakimova R, Hilburger MW, and Degenhardt R. Geometric imperfections and lower-bound methods used to calculate knock-down factors for axially compressed composite cylindrical shells. *Thin-Walled Structures*, 74:118–132, 1 2014. [Online; accessed 2024-04-09].
- [2] Lee A, López Jiménez F, Marthelot J, Hutchinson JW, and Reis PM. The Geometric Role of Precisely Engineered Imperfections on the Critical Buckling Load of Spherical Elastic Shells. *Journal of Applied Mechanics*, 83(11), sep 1 2016. [Online; accessed 2024-04-09].
- [3] Medina E, Farrell PE, Bertoldi K, and Rycroft CH. Navigating the landscape of nonlinear mechanical metamaterials for advanced programmability. *Physical Review B*, 101(6), feb 3 2020. [Online; accessed 2024-04-09].

- [4] Shen J, Garrad M, Zhang Q, Leao O, Pirrera A, and Groh RMJ. Active reconfiguration of multistable metamaterials for linear locomotion. *Physical Review B*, 107(21), jun 15 2023. [Online; accessed 2024-04-09].
- [5] Shen J, Pirrera A, and Groh RMJ. Building blocks that govern spontaneous and programmed pattern formation in pre-compressed bilayers. *Proceedings of the Royal Society A: Mathematical, Physical and Engineering Sciences*, 478(2265), 9 2022. [Online; accessed 2024-04-09].
- [6] Meeussen AS, Oğuz EC, Shokef Y, and van Hecke M. Topological defects produce exotic mechanics in complex metamaterials. *Nature Physics*, 16(3):307–311, jan 27 2020. [Online; accessed 2024-04-09].
- [7] Virgin L. Simultaneous Buckling, Contact, and Load-Carrying Capacity. *Journal of Engineering Mechanics*, 147(5), 5 2021. [Online; accessed 2024-04-09].
- [8] Zhang Y, Shen J, Yan Y, Tong J, Zhang L, and Liu Y. Enhancing the mobility of small-scale robots via nonlinear structural springs exhibiting negative stiffness. *Journal of Applied Mechanics*, 2024. Accepted.
- [9] Pirrera A, Avitabile D, and Weaver PM. Bistable plates for morphing structures: A refined analytical approach with high-order polynomials. *International Journal of Solids and Structures*, 47(25-26):3412–3425, 12 2010. [Online; accessed 2024-04-09].
- [10] Arena G, Groh RMJ, Brinkmeyer A, Theunissen R, Weaver PM, and Pirrera A. Adaptive compliant structures for flow regulation. *Proceedings of the Royal Society A: Mathematical, Physical and Engineering Sciences*, 473(2204):20170334, 8 2017. [Online; accessed 2024-04-09].
- [11] Wheatcroft ED, Shen J, Groh RMJ, Pirrera A, and Schenk M. Structural function from sequential, interacting elastic instabilities. *Proceedings of the Royal Society A: Mathematical, Physical and Engineering Sciences*, 479(2272), 4 2023. [Online; accessed 2024-04-09].
- [12] Shen J, Garrad M, Zhang Q, Wong V, Pirrera A, and Groh RMJ. A rapid-response soft end effector inspired by the hummingbird beak. *Journal of the Royal Society Interface*, 2024. (Under review).
- [13] Mang HA, Schranz C, and Mackenzie-Helnwein P. Conversion from imperfection-sensitive into imperfection-insensitive elastic structures I: Theory. *Computer Methods in Applied Mechanics and Engineering*, 195(13-16):1422–1457, 2 2006. [Online; accessed 2024-04-09].
- [14] Schranz C, Krenn B, and Mang HA. Conversion from imperfection-sensitive into imperfection-insensitive elastic structures. II: Numerical investigation. *Computer Methods in Applied Mechanics and Engineering*, 195(13-16):1458–1479, 2 2006. [Online; accessed 2024-04-09].
- [15] Ning X and Pellegrino S. Imperfection-insensitive axially loaded thin cylindrical shells. *International Journal of Solids and Structures*, 62:39–51, 6 2015. [Online; accessed 2024-04-09].
- [16] White SC and Weaver PM. Towards imperfection insensitive buckling response of shell structures-shells with plate-like post-buckled responses. *The Aeronautical Journal*, 120(1224):233–253, 2 2016. [Online; accessed 2024-04-09].
- [17] Hu N, Burgueño R, and Lajnef N. Structural Optimization and Form-Finding of Cylindrical Shells for Targeted Elastic Postbuckling Response. In *Volume 1: Development and Characterization of Multifunctional Materials; Modeling, Simulation and Control of Adaptive Systems; Structural Health Monitoring; Keynote Presentation.* American Society of Mechanical Engineers, sep 8 2014. [Online; accessed 2024-04-09].
- [18] Liguori FS, Madeo A, Magisano D, Leonetti L, and Garcea G. Post-buckling optimisation strategy of imperfection sensitive composite shells using Koiter method and Monte Carlo simulation. *Composite Structures*, 192:654–670, 5 2018. [Online; accessed 2024-04-09].
- [19] Cox BS, Groh RMJ, Avitabile D, and Pirrera A. Modal nudging in nonlinear elasticity: Tailoring the elastic post-buckling behaviour of engineering structures. *Journal of the Mechanics and Physics of Solids*, 116:135–149, 7 2018. [Online; accessed 2024-04-09].
- [20] Cox BS, Groh RMJ, and Pirrera A. Nudging Axially Compressed Cylindrical Panels Toward Imperfection Insensitivity. *Journal of Applied Mechanics*, 86(7), apr 19 2019. [Online; accessed 2024-04-09].
- [21] Groh RMJ, Avitabile D, and Pirrera A. Generalised path-following for well-behaved nonlinear structures. *Computer Methods in Applied Mechanics and Engineering*, 331:394–426, 4 2018. [Online; accessed 2024-04-09].
- [22] Roorda J and Chilver AH. Frame buckling: An illustration of the perturbation technique. *International Journal of Non-Linear Mechanics*, 5(2):235–246, 6 1970. [Online; accessed 2024-04-09].
- [23] Riks E. The Application of Newton's Method to the Problem of Elastic Stability. *Journal of Applied Mechanics*, 39(4):1060–1065, dec 1 1972. [Online; accessed 2024-04-09].
- [24] Akima H. A New Method of Interpolation and Smooth Curve Fitting Based on Local Procedures. *Journal of the ACM*, 17(4):589–602, 10 1970. [Online; accessed 2024-05-30].